Fermilab

DESI 2024: Constraints on Physics-Focused Aspects of Dark Energy using DESI DR1 BAO Data

FERMILAB-PUB-24-0756-PPD

arXiv:2405.13588

arXiv:2405.13588v2 [astro-ph.CO] 30 May 2024

DESI 2024: Constraints on Physics-Focused Aspects of Dark Energy using DESI DR1 BAO Data

K. Lodha[1,2] A. Shafieloo[1,2] R. Calderon[1] E. Linder[3,4,5]
W. Sohn[1] J. L. Cervantes-Cota[6] A. de Mattia[7]
J. García-Bellido[8] M. Ishak[9] W. Matthewson[1] J. Aguilar[3]
S. Ahlen[10] D. Brooks[11] T. Claybaugh[3] A. de la Macorra[12]
A. Dey[13] B. Dey[14] P. Doel[11] J. E. Forero-Romero[15,16]
E. Gaztañaga[17,18,19] S. Gontcho A Gontcho[3] C. Howlett[20]
S. Juneau[13] S. Kent[21,22] T. Kisner[3] A. Kremin[3]
A. Lambert[3] M. Landriau[3] L. Le Guillou[23] P. Martini[24,25,26]
A. Meisner[13] R. Miquel[27,28] J. Moustakas[29]
J. A. Newman[14] G. Niz[30,31] N. Palanque-Delabrouille[7,3]
W. J. Percival[32,33,34] C. Poppett[3,4,5] F. Prada[35] G. Rossi[36]
V. Ruhlmann-Kleider[7] E. Sanchez[37] E. F. Schlafly[38]
D. Schlegel[3] M. Schubnell[39,40] H. Seo[41] D. Sprayberry[13]
G. Tarlé[40] B. A. Weaver[13] H. Zou[42]

Affiliations are in Appendix C

E-mail: kushallodha@kasi.re.kr, shafieloo@kasi.re.kr

Abstract. Baryon acoustic oscillation data from the first year of the Dark Energy Spectroscopic Instrument (DESI) provide near percent-level precision of cosmic distances in seven bins over the redshift range $z = 0.1$–4.2. We use this data, together with other distance probes, to constrain the cosmic expansion history using some well-motivated physical classes of dark energy. In particular, we explore three physics-focused behaviors of dark energy from the equation of state and energy density perspectives: the thawing class (matching many simple quintessence potentials), emergent class (where dark energy comes into being recently, as in phase transition models), and mirage class (where phenomenologically the distance to CMB last scattering is close to that from a cosmological constant Λ despite dark energy dyAll three classes fit the data at least as well as ΛCDM, and indeed can improve on it by $\Delta\chi^2 \approx -5$ to -17 for the combination of DESI BAO with CMB and supernova data, while having one more parameter. The mirage class does essentially as well as $w_0 w_a$CDM while having one less parameter. These classes of dynamical behaviors highlight worthwhile avenues for further exploration into the nature of dark energy.

Contents

1 Introduction

Cosmic distances and the cosmic expansion rate contain information on the matter and energy contents of the universe. Redshift surveys can measure these at many epochs in cosmic history and so are especially valuable in separating the contributions and studying their evolution. In particular, a central question in cosmology is the nature of cosmic acceleration: does it originate from a cosmological constant Λ or a dynamically evolving dark energy?

Dark energy can be explored through the use of particular models, general parametrizations, or in a model-independent manner. In the absence of a fundamental theory pointing to a compelling model, and for robustness, many analyses take one of the latter two routes. The standard parametrization for the dark energy equation of state $w(a) = w_0 + w_a(1 - a)$ originated from exact solutions of the dark energy physical dynamics and has been demonstrated to be accurate to $\sim 0.1\%$ [1, 2] in matching distances and expansion rates over a wide array of models. Results for $w_0 w_a$CDM cosmology using DESI data are presented in [3]. Model-independent or at least model-agnostic approaches, e.g. Crossing Statistics, Gaussian Processes, values in redshift bins, etc., are investigated in [4] and forthcoming works for DESI data.

Here, we take a middle path, with general parametrizations informed by physics properties. Thus we do not use specific models, but are focused by the physics into classes of dynamical evolution. One perspective is to address the evolution in terms of the dark energy equation of state, specifically the thawing class, and another in terms of the dark energy density, specifically where dark energy arises quickly, whether through a phase transition or

a rapid growth ($w \ll -1$). A third class is the mirage class [5], where an apparent $w = -1$ when forced to a constant value actually hides dynamics. These are chosen because previous data pointed to these physical properties as compatible with observations, at least as well as the cosmological constant, and they describe broad classes of characteristic behavior, rather than a single model.

New, highly precise data have become available from Data Release 1 of the DESI baryon acoustic oscillations (DESI BAO) measurements. The data are discussed in detail in [3, 6, 7]. Here we investigate their implications for the dark energy physics, using the physics-focused classes above. Section 2 describes the physics-focused classes for the dark energy equation of state and density. In Section 3 we review the DESI distance data in seven redshift ranges, as well as other data sets used in combination. Constraints on cosmology and the physics implications are discussed in Section 4, with conclusions in Section 5.

2   Physics-focused classes

The current data, including DESI BAO, favors dynamical dark energy over a simple cosmo-logical constant at various levels of significance when different data set combinations are used, as shown in [3]. This motivates consideration of a wide variety of dark energy behaviors.

However, there is no compelling physics-based theory for dark energy differing from Λ, so one tends to adopt a more phenomenological approach. Here, we want to retain physics to a significant extent and use classes of dark energy properties consistent with the data, and that are more general than specific models.

Dark energy properties enter the measurements through their impact on cosmic distances (we do not here consider growth probes of large scale structures). This follows from the Friedmann equations, and we can write the dark energy influence as (assuming a spatially flat universe)

$$\frac{H^2(z)}{H_0^2} = \Omega_{\rm m,0}(1+z)^3 + \Omega_{\rm r,0}(1+z)^4 + (1 - \Omega_{\rm m,0} - \Omega_{\rm r,0})\, f_{\rm DE}(z) \;, \qquad (2.1)$$

where $\Omega_{\rm m,0}$ and $\Omega_{\rm r,0}$ are the present fractions of the critical energy density in matter and radiation respectively, and $f_{\rm DE}(z)$ describes the dark energy density evolution. The dark energy equation of state, or pressure to energy density ratio, then comes from the continuity equation as

$$w(z) = -1 + \frac{1}{3}\frac{d \ln f_{\rm DE}(z)}{d \ln (1 + z)} \;. \qquad (2.2)$$

For example,

$$w(a) = w_0 + w_a(1 - a) \quad \Leftrightarrow \quad f_{\rm DE}(a) = a^{-3(1+w_0+w_a)}\, e^{-3w_a(1-a)} \;, \qquad (2.3)$$

where the scale factor $a = 1/(1 + z)$. The key then is seeing how physics informs the dark energy density $f_{\rm DE}(z)$ or equation of state $w(a)$. We assume throughout that the dark energy fluid sound speed $c_s^2 = 1$.

2.1   Dark Energy Equation of State: Thawing Physics

While writing the dark energy equation of state as $w(a) = w_0 + w_a(1 - a)$ [1, 8] has been shown to be highly accurate for a wide variety of models [1, 2], the physics does not actually

predict that any *arbitrary* combination of w_0 and w_a is equally valid. Basic physics – evolution of the dark energy field through the long history of radiation and matter domination in the presence of Hubble friction – calls out two regions of the phase space as preferred, known as the thawing and freezing regions [9]. Other regions of the phase space arise only due to extraordinary circumstances, e.g. fine tuning, noncanonical kinetic structure, or nongravitational interactions. The freezing region, with $w_a > 0$, tends not to be compatible with observations; indeed DESI BAO plus other probes disfavors it at $\sim 3\sigma$ [3]. Thus we focus on exploring the thawing physics class.

Thawing physics arises because, during the long cosmic history, the Hubble friction was high enough to overcome dark energy dynamics, causing it to act like a cosmological constant. Only recently, as the Hubble expansion rate declined sufficiently, was dark energy released to allow dynamics ("thawed"). This describes a broad variety of particle physics models for dark energy, including pseudo-Nambu-Goldstone bosons (PNGB [10]; e.g. axions), the linear potential [11] with its shift symmetry shielding against quantum corrections, and many monomial potentials (e.g. the standard quadratic $V \sim m^2\phi^2$ and quartic $V \sim \lambda\phi^4$).

One of the great virtues of the w_0–w_a parametrization is that it acts as a calibration relation for the physics. Not only are the thawing fields in the same class, but w_0–w_a calibrates their evolution $w(a)$, bringing their phase space tracks in w–w' into a universal relation [2]:

$$w_a \approx -1.58(1 + w_0) \ . \tag{2.4}$$

(The coefficient -1.58 comes from fits to the dynamics in [2], e.g. see Eq. (1) of [12].)

Another approach to thawing dynamics is to account for the Hubble friction freeze in the past plus an algebraic factor describing the thawing, roughly related to the ratio of the frozen dark energy density to the matter density, $\sim a^3$. Again, these are general characteristics of the thawing class as a whole, and so not model dependent in the usual sense. Following [12, 13] we have

$$1 + w(a) = (1 + w_0)\, a^3 \left(\frac{3}{1 + 2a^3}\right)^{2/3} \ . \tag{2.5}$$

Note that both the calibration and algebraic forms have simply one parameter more than ΛCDM. They have also both been demonstrated to have accuracy better than 0.1% in matching distances $d(z)$ and Hubble expansion rates $H(z)$ of the exact physics [12]. Describing the thawing class by either the calibration or algebraic forms gives virtually identical results (see Fig. 7 in Appendix A), adding support for the model-independent nature of the analysis.

2.2 Dark Energy Density: Emergent Physics

In contrast to the previous subsection, we now consider the dark energy density, rather than the equation of state, and a rapid emergence or transition rather than a slow thaw. In this class of physical behavior, dark energy is negligible (or vanishes) above moderate redshift (say $z \approx 2$) but its energy density quickly grows at lower redshift (implying $w < -1$) before leveling off to a constant in the future (and so $w \to -1$). Physical examples of this behavior include phase transitions such as vacuum metamorphosis [14, 15] and dark energy as a critical phenomena [16, 17]. The density of dark energy as a critical phenomenon can behave similarly to the magnetization of the Ising model and effectively emerges at a particular time (redshift) corresponding to the critical temperature in the model [17].

Phenomenological Emergent Dark Energy (PEDE) model [18, 19] has been introduced as a zero freedom dark energy model where dark energy has no effective presence in the past

and effectively emerges in the late Universe. The model was generalised as Generalised Emergent Dark Energy (GEDE) [20], to include both PEDE and Λ as two limits of the parametric form and to include a larger class of emergent dark energy behaviors.

The evolution of the energy density in GEDE is given by [20, 21]

$$f_{\rm DE}(z) = \frac{1 - \tanh\left(\Delta \times \log_{10}(\frac{1+z}{1+z_t})\right)}{1 + \tanh\left(\Delta \times \log_{10}(1+z_t)\right)} \; , \tag{2.6}$$

where Δ is a free parameter, determining the steepness of the transition, and z_t is a derived quantity determined by solving $\rho_m(z_t) = \rho_{\rm DE}(z_t)$. The corresponding equation of state for GEDE is

$$w(z) = -1 - \frac{\Delta}{3\ln(10)}\left[1 + \tanh\left(\Delta \log_{10}\left(\frac{1+z}{1+z_t}\right)\right)\right] \; . \tag{2.7}$$

Note that $f_{\rm DE}(z)$ goes from much less than one for $z \gg z_t$ to one today to a finite value greater than one in the future (de Sitter state), while $w(z)$ goes from $-1 - 2\Delta/(3\ln 10)$ at $z \gg z_t$ to -1 in the future.

2.3 Dark Energy: Mirage Physics

Another, more phenomenological class is that of mirage dark energy [5]. This originated as a way to match the CMB distance to last scattering from ΛCDM but for some evolving dark energy equation of state $w(a)$. More generally, it will appear to yield a constant $w = -1$ for data combinations with a pivot point, or greatest sensitivity to dark energy equation of state, around $a \approx 0.7$. The condition becomes

$$w_a = -3.66\,(1 + w_0) \; . \tag{2.8}$$

(The coefficient -3.66 comes from Eqs. (1) and (3) of [5] and varies by a couple percent over the range $\Omega_{\rm m,0} \in [0.25, 0.35]$.)

Interestingly, DESI BAO DR1 gives a confidence contour in the w_0–w_a plane that follows this closely, and indeed delivers a $w \approx -1$ fit when assuming $w = {\rm const}$ (e.g. see Fig. 5 of [3]). We emphasize, however, as demonstrated in this article and [4], that this does not actually mean that $w = {\rm const}$. That may merely be a mirage, even for quite rapidly evolving $w(a)$. Note furthermore that since mirage models match the CMB distance, they will also generally closely match the growth of structure (within general relativity), as the mirage holds for this as well (see [22] and Fig. 6 of [5] for demonstration).

As to the physical mechanism behind the mirage, this is less clear. Such a crossing of $w(a) = -1$ is a hallmark of perhaps a combination of multiple scalar fields, interactions, or modified gravity generally involving noncanonical kinetic terms and possibly braiding of the scalar and tensor degrees of freedom. Rapid emergence of the dark energy density (i.e. strongly negative w_a and hence $w(a) \ll -1$ at early redshifts) however is not a generic characteristic of such mechanisms, and if taken at face value could point more to a phase transition mechanism. Many of those, however, such as vacuum metamorphosis [14], tend toward a de Sitter ($w = -1$) state not $w_0 > -1$. It is not clear what reasonable physics would contain both a rapid emergence in density and a crossing of $w(a) = -1$. (Speculatively, one could imagine the scalar field responsible for the phase transition having a negative potential or some interaction that would cause crossing of $w(a) = -1$.)

Table 1. Parameters and priors used in the analysis with our modified version of the Boltzmann solver `class`. All of the priors are uniform in the ranges specified below.

	parameter	prior/value
background-only	$\Omega_{m,0}$	$\mathcal{U}[0.01, 0.99]$
	$H_0 r_d \, [\, \mathrm{km \, s^{-1}}]$	$\mathcal{U}[1000, 100000]$
CMB	$\omega_{cdm} \equiv \Omega_{cdm} h^2$	$\mathcal{U}[0.001, 0.99]$
	$\omega_b \equiv \Omega_b h^2$	$\mathcal{U}[0.005, 0.1]$
	$\ln(10^{10} A_s)$	$\mathcal{U}[1.61, 3.91]$
	n_s	$\mathcal{U}[0.8, 1.2]$
	$H_0 \, [\, \mathrm{km \, s^{-1} \, Mpc^{-1}}]$	$\mathcal{U}[20, 100]$
	τ	$\mathcal{U}[0.01, 0.8]$
Thawing/Mirage	w_0	$\mathcal{U}[-3, 1]$
GEDE	Δ	$\mathcal{U}[-3, 10]$
$w_0 w_a$	w_0	$\mathcal{U}[-3, 1]$
	w_a	$\mathcal{U}[-3, 2]$

3 Data and Methodology

The cosmological probes and specific data sets used in our analysis are:

- **Baryon Acoustic Oscillations (BAO):** We use the compilation of compressed distance quantities D_M/r_d, D_H/r_d, and D_V/r_d from the first year data release of the Dark Energy Spectroscopic Instrument [23–27], where D_M is the transverse comoving distance, D_H the Hubble distance, D_V their isotropic average, and r_d is the sound horizon at the baryon drag epoch. This dataset, abbreviated as "DESI BAO", spans seven redshift bins from $z = 0.3$ to $z = 2.33$ [6]. We refer the reader to [3, 6, 7, 27–30] for further details.

- **Supernovae Ia (SNe Ia):** We combine with supernova data from three sets, one at a time: "PantheonPlus", a compilation of 1550 supernovae spanning a redshift range from 0.01 to 2.26 [31], "Union3", containing 2087 SNe Ia processed through the Unity 1.5 pipeline based on Bayesian Hierarchical Modelling [32], and "DES-SN5YR", a compilation of 194 low-redshift SNe Ia ($0.025 < z < 0.1$) and 1635 photometrically classified SNe Ia covering the range $0.1 < z < 1.3$ [33].

- **Cosmic Microwave Background (CMB):** We also include temperature and polarization measurements of the CMB from the Planck satellite [34]. In particular, we use the high-ℓ TTTEEE likelihood (`planck_2018_highl_plik.TTTEEE`), together with low-ℓ TT (`planck_2018_lowl.TT`) and low-ℓ EE (`planck_2018_lowl.EE`) [35], as implemented in `cobaya` [36]. Additionally, we include CMB lensing measurements from the combination of NPIPE PR4 from Planck [37] and the Atacama Cosmology Telescope (ACT DR6) [38, 39] using importance sampling. When using the combined Planck+ACT lensing likelihood, we use `accurate_lensing:1` and `delta_l_max:800` options to match CAMB precision settings as recommended by ACT.

In our analysis, we utilize Markov Chain Monte Carlo (MCMC) sampling to explore the parameter space using the Metropolis-Hastings algorithm [40, 41] as implemented in

cobaya [36]. To facilitate efficient sampling of the CMB Planck likelihoods, we employ the "fast-dragging" scheme [42]. We have adopted priors similar to [3], as presented in Table 1, and have modified the Boltzmann solver `class` [43, 44] incorporating a generalized equation of state for dark energy for the theoretical prediction of observables. We switched to the `Recfast` option for recombination as it does not assume anything about the equation of state. We assume three neutrino species with $\sum m_\nu = 0.06$ eV and $N_{\rm eff} = 3.044$. For the supernovae likelihoods (PantheonPlus, Union3, and DES-SN5YR), we analytically marginalize over the absolute magnitude M_B. For clarity of presentation, in the main text figures we use PantheonPlus but list constraints from each supernova set in the tables and show their contours in Appendix B.

4 Results and Discussions

We present the results for each class in turn, showing the cosmological parameter joint posteriors and the reconstructed dark energy equation of state $w(z)$ and energy density $f_{\rm DE}(z)$ for various combinations of data sets.

4.1 Thawing

Figure 1 shows the joint parameter constraints for the thawing class. The dashed black line corresponds to ΛCDM ($w_0 = -1$). In the first few rows of Table 2, we report the marginalized constraints on some of the relevant cosmological parameters and for various data combinations. The addition of CMB data to DESI BAO significantly reduces the uncertainty in w_0, shifting its value to < -1, which also results in $w_a > 0$. However, combining DESI BAO with PantheonPlus yields $w_0 > -1$. A combination of all three datasets provides even tighter constraints, with posteriors peaking at $w_0 \gtrsim -1$, hence $w_a < 0$. Using either of the other two supernova datasets instead somewhat strengthens $w_0 > -1$. Figure 2 illustrates the behaviors for the equation of state $w(z)$ and energy density evolution $f_{\rm DE}(z)$.

We emphasize that the relations $w_a(w_0)$ for both the thawing and mirage classes are designed to replicate *observations*, i.e. distances and Hubble parameters to $\sim 0.1\%$, not the actual $w(z)$ for a specific model within the class, and hence do not need to have $w(z \gg 1) \to -1$, say. Indeed $w(z)$ can appear to cross -1 even if it actually doesn't, yet still fit the observations exquisitely – this is well known: see Table 1 of [12] and Fig. 14 of [45] for a PNGB model, [46] for a hilltop model, etc. However, for $|w_a| \gtrsim 1$ such unreal crossings of $w(z) = -1$ tend to be in conflict with the CMB distance to last scattering, and such strong crossings tend in fact to be real.

4.2 Generalized Emergent Dark Energy

The GEDE analysis proceeds similarly, with Fig. 3 showing its constraints on parameters, using the same datasets. When considering DESI BAO alone, the dataset is broadly consistent with $\Delta = 0$, corresponding to ΛCDM. However, when combined with CMB, Δ peaks at a positive value ($\Delta \simeq 1$, corresponding to PEDE [18]), indicating that dark energy emerges at late times. Adding PantheonPlus, GEDE prefers a negative value of Δ, which corresponds to the injection of energy at earlier redshifts. However, combining all three datasets results in a peak near $\Delta = 0$, indicating that dark energy density remains roughly constant throughout evolution and that GEDE is not preferred over ΛCDM. Note that the model-agnostic reconstructions of dark energy in [4] do seem to indicate a sharp emergence of dark energy in the recent past. The issue is that GEDE sharply emerges, but asymptotes to $w = -1$ rather
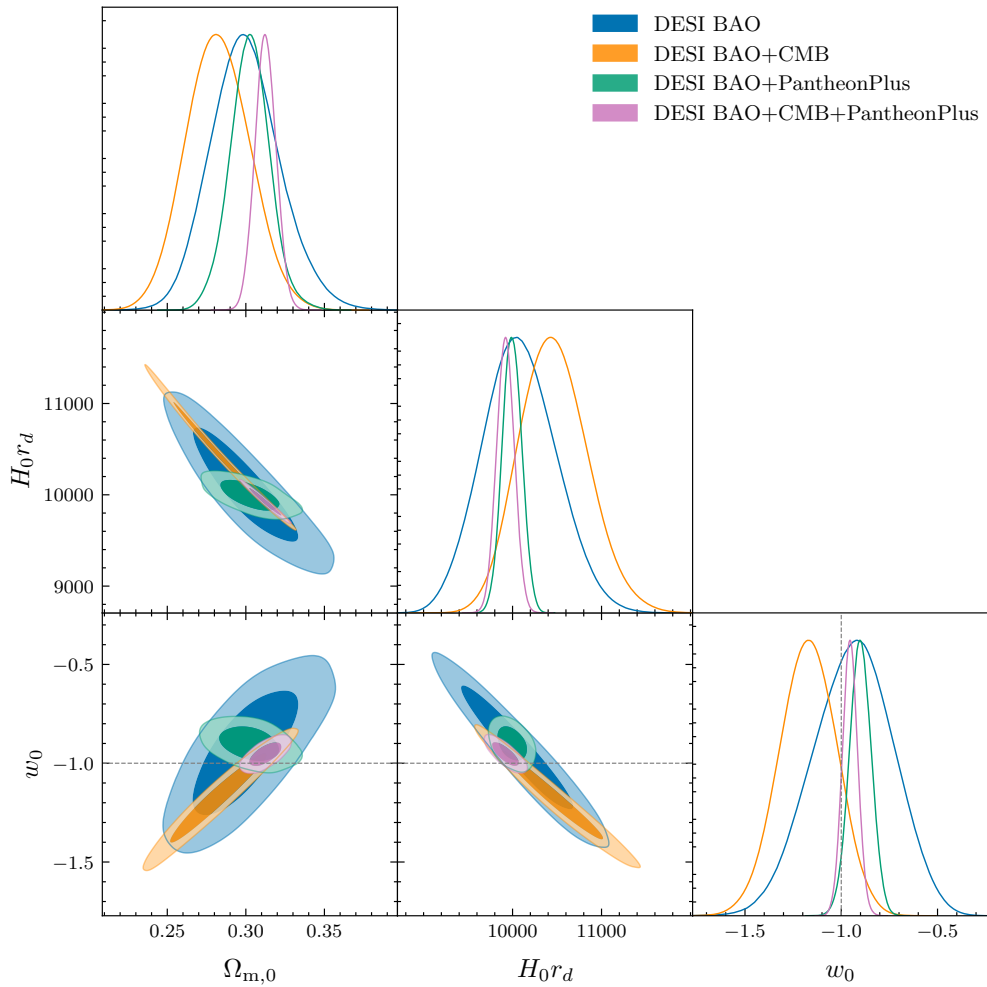
Figure 1. Marginalized constraints within the thawing class of dark energy described by Eq. (2.4), from different combinations of data sets.
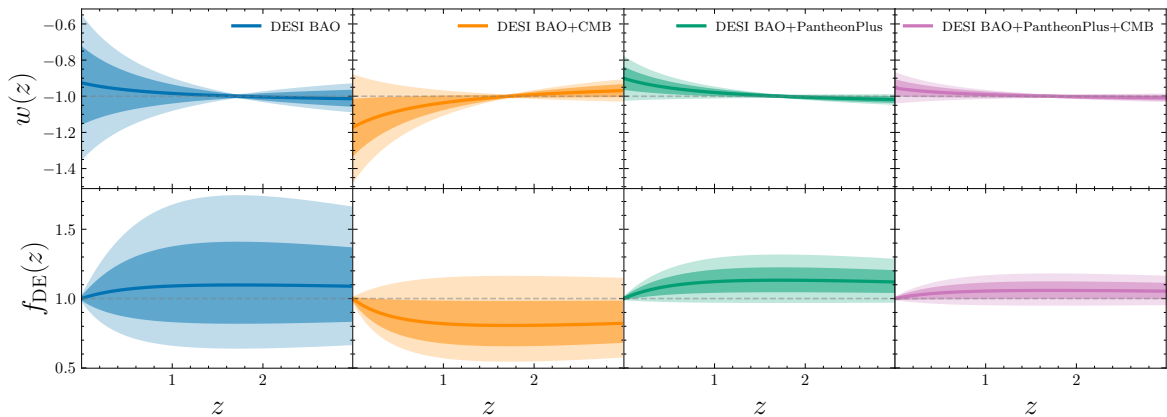
Figure 2. Marginalized constraints on the dark energy equation of state $w(z)$ and energy density $f_{\mathrm{DE}}(z)$ for the thawing class, parametrized by Eq. (2.4).

than crossing it. Increasing Δ fits the $z \approx 1$ data better than ΛCDM but the $z \lesssim 0.5$ data prefers $w > -1$ and so GEDE is worse than ΛCDM there, resulting in GEDE "mellowing" to approach ΛCDM behavior (and so, as we will see, not having a particularly advantageous goodness of fit). If there were an emergent model that also crossed $w = -1$ then this might provide a superior fit to data, but physics motivation for such behavior is not obvious. Figure 4 exhibits the uncertainty bands for the reconstructed equation of state $w(z)$ and energy density evolution $f_{\mathrm{DE}}(z)$.
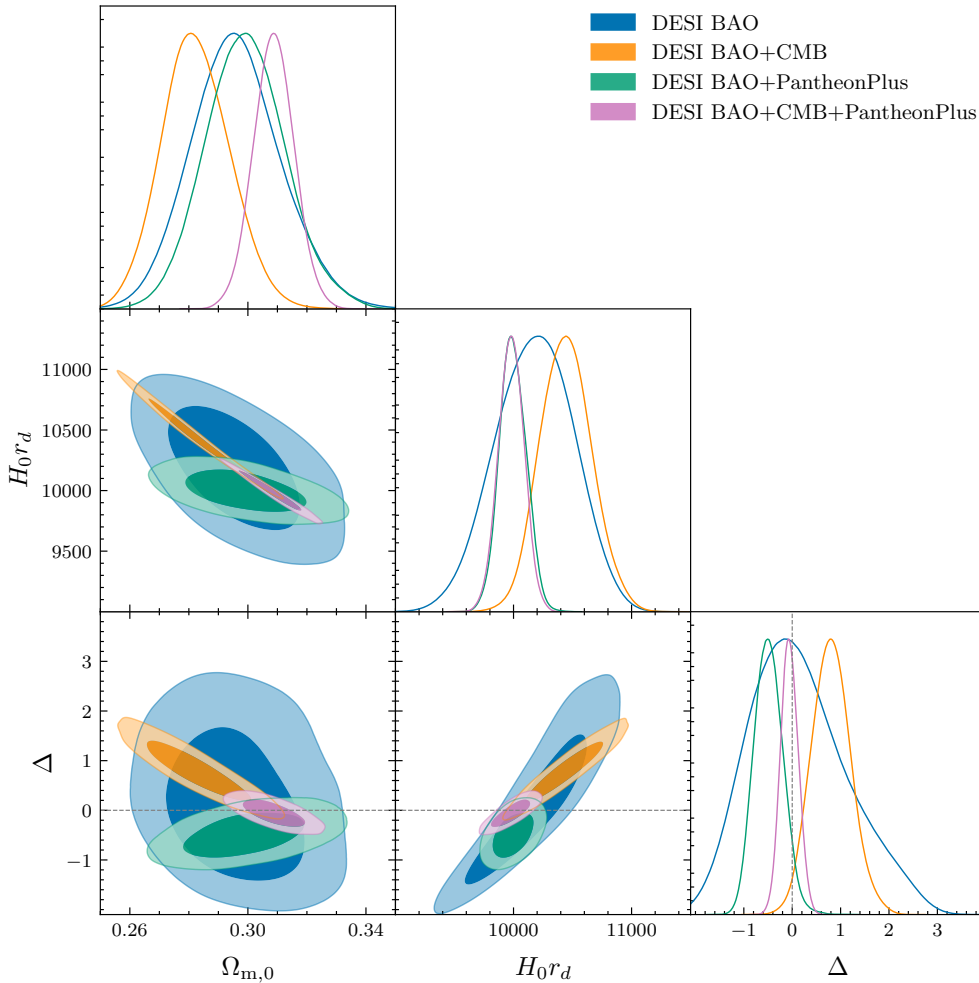
Figure 3. Marginalized constraints within the Generalized Emergent Dark Energy (GEDE) class described by Eq. (2.6).

4.3 Mirage

The mirage class has cosmological parameter constraints illustrated in Fig. 5. Again, the preference is pulled off ΛCDM (which is a member of this class, where the mirage is real). A best fit of $w_0 \approx -0.8$, and hence $w_a \approx -0.7$, is quite consistent with DESI BAO data, including in combination with other data sets such as CMB and supernovae. One can make w_0 even less negative (and hence w_a more negative), i.e. strengthen the mirage, if one compensates by decreasing the late time dark energy density (increasing $\Omega_{\mathrm{m},0}$), as seen in Fig. 5.
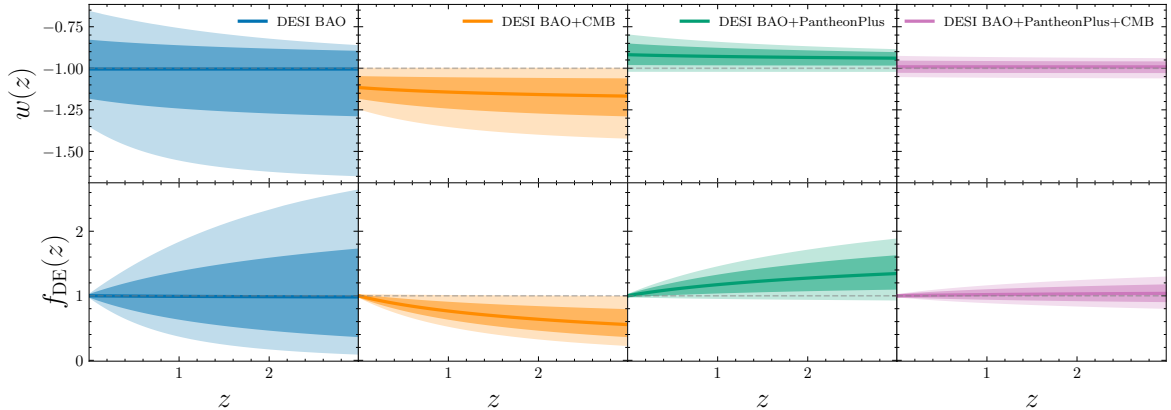
Figure 4. Marginalized constraints on the dark energy equation of state $w(z)$ and energy density $f_{\rm DE}(z)$ for the GEDE model, parametrized by Eq. (2.6).

At earlier times, the strongly negative w_a implies a strongly negative $w(a)$, and hence very little dark energy density, before rapidly increasing in energy density while crossing $w(a) = -1$. This effectively is acting like GEDE at higher redshift and the thawing class at lower redshift. In Figure 6, we show the reconstructed equation of state $w(z)$, crossing the $w = -1$ threshold near $z \approx 0.4$, along with the corresponding evolution of energy density $f_{\rm DE}(z)$; these results agree with the DESI results in [3, 4].

4.4 Comparison and Discussion

Table 2 summarizes the constraints on relevant cosmological parameters. One general aspect to note is that the clustering amplitude parameter S_8 has a rather consistent and reasonable value for all three classes (note that no direct galaxy clustering growth data is used, only BAO). When combining all three cosmological probes, the values of H_0 and $\Omega_{\rm m}$ are also quite consistent both across classes and regardless of which supernova dataset is included. For the thawing class, w_0 is pulled somewhat off Λ. For GEDE, Δ is mostly consistent with zero (hence Λ). The mirage class is where the strongest deviation from Λ is seen, and as we discuss next is where the goodness of fit is best as well. Consistency between a class and ΛCDM should be viewed not through the 1D confidence intervals, however, but through the joint parameter constraints and the $\Delta\chi^2$ quantification.

Table 3 presents how the three classes compare to each other, relative to ΛCDM, and w_0w_aCDM in goodness of fit ($\Delta\chi^2$), for various combinations of datasets. Here, we report $\Delta\chi^2_{\rm MAP}$, the difference between the maximum a posteriori of the model and the maximum of the posterior fixing $w_0 = -1$ or $\Delta = 0$ (i.e. to the cosmological constant case). Note that the three classes have one more parameter than ΛCDM and one less than w_0w_aCDM. The first general result of interest is that all three classes have better χ^2 than ΛCDM. They do have one more parameter but in the combination of all three cosmological probes, the improvement is notably more than one. Note that w_0w_aCDM has a significantly better χ^2 than ΛCDM, even taking into account its two more parameters, as discussed in [3]. However, the χ^2 for the physics-focused classes are often close to the w_0w_aCDM values, while having one less parameter. This is especially true for the mirage class, while the thawing class and GEDE appear to be less favored. As thawing and mirage are subsets of w_0w_aCDM, their χ^2 cannot go below that of w_0w_a; for the case of fitting DESI BAO data alone, this appears not to hold
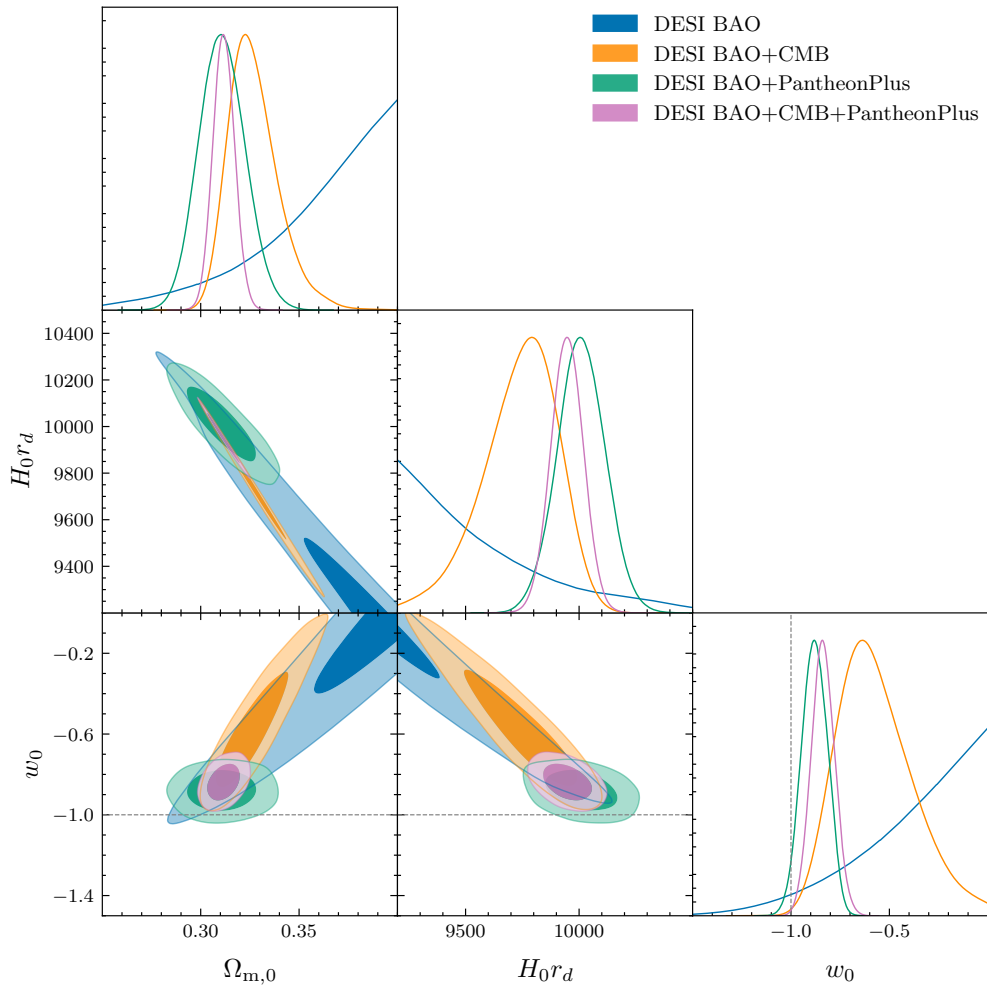
Figure 5. Marginalized constraints within the mirage class of dark energy described by Eq. (2.8).
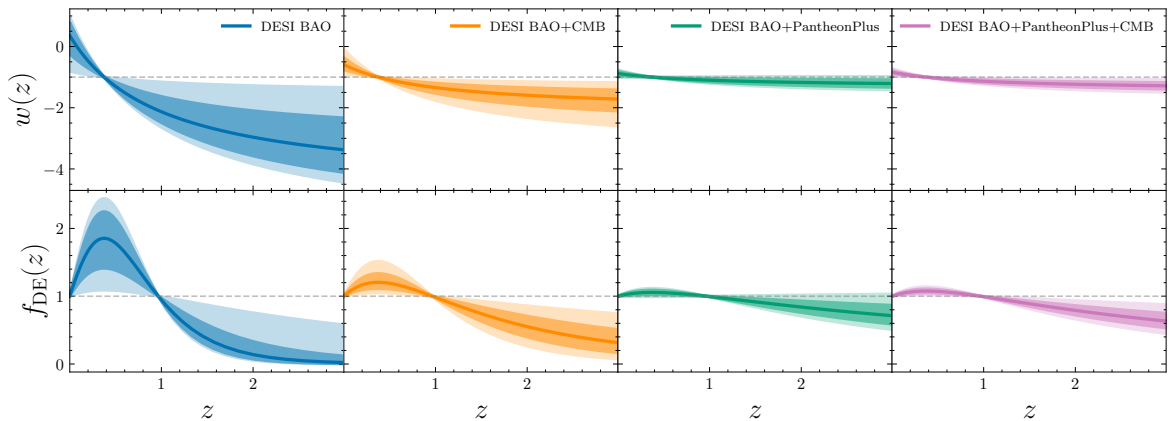
Figure 6. Marginalized constraints on the equation of state $w(z)$ for the mirage class, parametrized by Eq. (2.8).

Table 2. Constraints on the relevant cosmological parameters

Model/Dataset	$H_0[\mathrm{km\,s^{-1}\,Mpc^{-1}}]$	$\Omega_{\mathrm{m},0}$	w_0	Δ	S_8
Thawing					
DESI BAO+CMB	$71.0^{+2.4}_{-2.8}$	0.282 ± 0.020	-1.17 ± 0.15	$-$	0.812 ± 0.011
DESI BAO+CMB+Union3	66.55 ± 0.95	0.3195 ± 0.0094	-0.906 ± 0.060	$-$	0.8223 ± 0.0094
DESI BAO+CMB+DES-SN5YR	66.49 ± 0.61	0.3200 ± 0.0065	-0.902 ± 0.038	$-$	0.8224 ± 0.0091
DESI BAO+CMB+PantheonPlus	67.31 ± 0.66	0.3125 ± 0.0067	-0.954 ± 0.040	$-$	0.8208 ± 0.0092
GEDE					
DESI BAO+CMB	71.0 ± 1.5	0.282 ± 0.012	$-$	0.81 ± 0.40	0.8156 ± 0.0092
DESI BAO+CMB+Union3	$67.6^{+1.0}_{-0.93}$	0.3096 ± 0.0089	$-$	-0.08 ± 0.25	0.8199 ± 0.0092
DESI BAO+CMB+DES-SN5YR	66.80 ± 0.69	0.3166 ± 0.0066	$-$	-0.28 ± 0.17	0.8207 ± 0.0091
DESI BAO+CMB+PantheonPlus	67.73 ± 0.74	0.3088 ± 0.0070	$-$	-0.06 ± 0.18	0.8198 ± 0.0093
Mirage					
DESI BAO+CMB	$66.2^{+1.3}_{-0.79}$	$0.3271^{+0.0093}_{-0.015}$	$-0.56^{+0.15}_{-0.23}$	$-$	0.842 ± 0.013
DESI BAO+CMB+Union3	66.67 ± 0.59	0.3217 ± 0.0072	$-0.657^{+0.096}_{-0.11}$	$-$	0.838 ± 0.010
DESI BAO+CMB+DES-SN5YR	67.10 ± 0.44	0.3169 ± 0.0056	-0.742 ± 0.066	$-$	0.8332 ± 0.0091
DESI BAO+CMB+PantheonPlus	67.55 ± 0.43	0.3117 ± 0.0055	-0.837 ± 0.060	$-$	0.8272 ± 0.0092

for the mirage class, but this is due to the limited prior range of $-3 < w_a < 2$ (also used for $w_0 w_a$ in [3]) – see the extended degeneracies in Fig. 5. When combining DESI BAO with other data this influence of the prior no longer matters.

The promising $\Delta\chi^2_{\mathrm{MAP}}$ for the mirage class led us to conduct additional nested-sampling runs using the `PolyChord` sampler [47] to calculate the Bayesian evidence using the `anesthetic` package [48]. We report the Bayes factors of $|\ln B_{21}| = 2.8$ (0.65), 4.2 (2.4), and 6.4 (2.8) in favor of the mirage class (compared to $w_0 w_a$CDM) over ΛCDM for the DESI+CMB with PantheonPlus, Union3, and DES-SN5YR data combinations, respectively. These findings suggest a moderate preference for the mirage class over ΛCDM by the PantheonPlus combination and a strong preference by the Union3 and DES-SN5YR on a Jeffreys' scale [49, 50].

Table 3. $\Delta\chi^2_{\mathrm{MAP}} \equiv \chi^2_{\mathrm{model}} - \chi^2_{\Lambda\mathrm{CDM}}$ values for the different models and data combinations. The minimum χ^2 values were obtained using `iminuit` [51] and `Py-BOBYQA` [52, 53] minimizer. Note that all data combinations include DESI BAO.

Data	$\Delta\chi^2_{\mathrm{Thawing}}$	$\Delta\chi^2_{\mathrm{GEDE}}$	$\Delta\chi^2_{\mathrm{Mirage}}$	$\Delta\chi^2_{w_0 w_a}$
DESI BAO	-0.2	-0.04	-5.0	-3.8
+CMB	-0.6	-5.7	-7.6	-8.9
+PantheonPlus	-3.2	-3.0	-3.5	-3.5
+Union3	-6.3	-5.2	-8.7	-8.9
+DES-SN5YR	-8.8	-7.7	-10.7	-11.1
+CMB+PantheonPlus	-0.6	-1.7	-9.0	-9.6
+CMB+Union3	-3.0	-3.2	-15.2	-15.6
+CMB+DES-SN5YR	-5.0	-4.8	-17.7	-18.3

5 Conclusion

Physics-focused classes can give insight into the nature of dynamical dark energy. Using DESI BAO data combined with different state-of-the-art supernovae compilations (PantheonPlus, Union3, DES-SN5YR) and CMB (Planck and ACT) observations, our main result indicates a preference for evolving dark energy rather than a cosmological constant. This behavior can be very well captured by the mirage class, evolving from $w < -1$ and low energy density at $z \gtrsim 1$ to $w > -1$ more recently. Note that this also gives a hump in the dark energy density at $z \approx 0.3$–0.5, in agreement with our previous model-agnostic findings [4]. The mirage class of dark energy models has a comparable $\Delta\chi^2$ with that of the $w_0 w_a$CDM model, while having one less degree of freedom.

The mirage class combines the emergence of dark energy density, perhaps indicative of a phase transition, with the recent evolution of $w(a)$ to less negative values than the cosmological constant of the thawing class. With DESI+SNe Ia, consistently across the three supernova sets, all three classes have better fits than ΛCDM and come close to $w_0 w_a$CDM (which has one more parameter). Neither thawing nor GEDE have a strong advantage for DESI+CMB, however, and the combination of all three cosmology probes gives a clear advantage to the mirage class over the other two (which are still better fits than ΛCDM). This preference is reflected in the Bayes factor, showing a moderate to strong preference (depending on the SNe Ia dataset considered) for the Mirage class over ΛCDM. However, the significance of the Bayesian evidences have to be interpreted cautiously [54, 55]. We leave a detailed model-selection analysis for future works.

Other cosmology parameters such as $H_0 r_d$, $\Omega_{\rm m}$, and S_8 remain near ΛCDM values when using any of the three classes with the full dataset combination. Together with model independent analyses, such physics-focused classes provide important clues to the physical properties we should seek in dark energy models, beyond the "blank slate" characterization of w_0–w_a.

The dark energy properties indicated by the data – consistent with [3, 4] – are rapid evolution from $w(a \ll 1) \ll -1$ across $w = -1$ to more recent $w(a \approx 1) > -1$, and hence emergent dark energy density at modest redshift while at low redshift an energy density bump together with a slowing down of recent cosmic acceleration (see e.g. the $q(z)$ reconstruction in [4]). These characteristics do not generally exist simultaneously in the usual dark energy models. Phase transition-type behavior does not generally give w evolving away from Λ today, and the thawing class evolving away from Λ today does not generally give $w < -1$, let alone $w \ll -1$, in the past.

If the data and its analysis hold, then we are facing a more complicated dark energy sector than generally treated, possibly involving multiple components or involving special nonlinearities in the action (modified gravity or couplings). Fortunately, further data is imminent, with more DESI BAO data, as well as DESI measurements of redshift space distortions and peculiar velocities that can test cosmic growth and gravity.

Data Availability

The data used in this analysis will be made public along the Data Release 1 (details in https://data.desi.lbl.gov/doc/releases/).

A Thawing Class: Calibration vs Algebraic Forms

The thawing class encompasses rich physics, including pseudo-Nambu Goldstone bosons (PNGB axions), the shift symmetric linear potential, and the classic ϕ^2 and ϕ^4 potentials. The calibration Eq. (2.4) and algebraic Eq. (2.5) forms were shown to accurately describe the exact numerical solutions for observables to $\sim 0.1\%$ (e.g. Table 1 of [12], and [2]). The former emphasizes the calibration, i.e. model independent, aspects of the physics, and the latter the dynamical evolution flow, but each captures the essential physics and Figure 7 confirms that the two forms give nearly identical results. The specific numbers quoted in this work use the calibration form.

Note that while the algebraic form Eq. (2.5) does not cross $w = -1$ while the calibration form Eq. (2.4) does, they both describe the *observations* nearly identically, with excellent accuracy. Thus not every $w(a)$ that crosses -1 indicates a physical crossing of -1; the forms are designed to describe the observations, not $w(a)$ itself, as emphasized in Section 4.1. However, for w_0 too far from -1, i.e. $|w_a|$ large enough, such apparent crossings will not fit certain observations like the distance to CMB last scattering, and so $|w_a| \gtrsim 1$ often does point to a real crossing of -1 by $w(a)$.
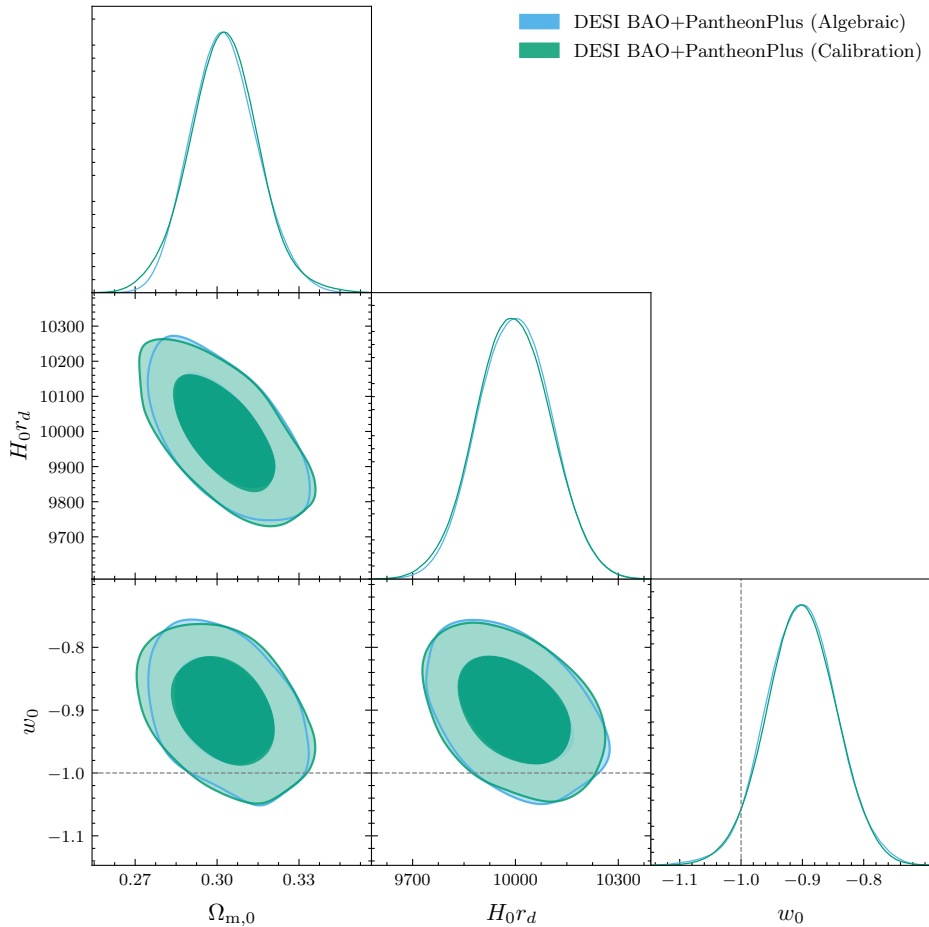
Figure 7. Comparison of the calibration Eq. (2.4) vs algebraic Eq. (2.5) parametrizations of the thawing class of dark energy, using DESI BAO+PantheonPlus.

B Supernova Data Comparison

The figures in the main section of the paper use PantheonPlus as the supernova dataset for clarity of presentation by limiting the number of contours. Tables 2 and 4 list the parameter constraints for each supernova dataset in turn. Here, Figure 8 presents the joint confidence contours using DESI BAO in combination with each supernova set in turn. The results are quite consistent between each supernova dataset and a similar trend can also be seen in Figure 6 of [3] for $w_0 w_a$CDM.

References

[1] E.V. Linder, *Exploring the expansion history of the universe*, *Phys. Rev. Lett.* **90** (2003) 091301 [astro-ph/0208512].

[2] R. de Putter and E.V. Linder, *Calibrating Dark Energy*, *JCAP* **10** (2008) 042 [0808.0189].

[3] DESI Collaboration, A.G. Adame, J. Aguilar, S. Ahlen, S. Alam, D.M. Alexander et al., *DESI 2024 VI: Cosmological Constraints from the Measurements of Baryon Acoustic Oscillations*, *arXiv e-prints* (2024) arXiv:2404.03002 [2404.03002].
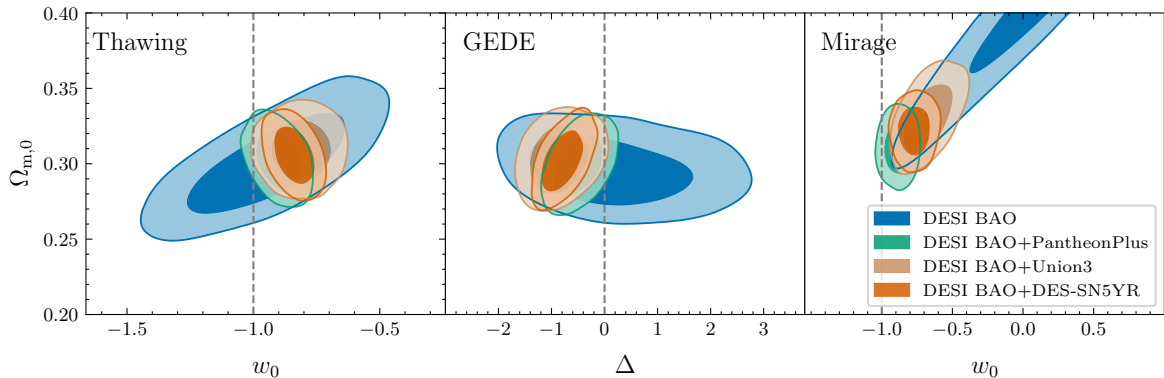
Figure 8. Marginalized posterior distributions using DESI BAO and each supernova dataset. The vertical dashed line indicates ΛCDM.

Table 4.   Constraints on the relevant cosmological parameters for DESI BAO and DESI BAO+SNe Ia datasets.

Model/dataset	$\Omega_{\mathrm{m},0}$	$H_0 r_d \,[\mathrm{km\,s^{-1}}]$	w_0	Δ
Thawing				
DESI BAO	$0.300^{+0.020}_{-0.023}$	10080 ± 410	-0.94 ± 0.20	–
DESI BAO+PantheonPlus	0.303 ± 0.013	9994 ± 110	-0.901 ± 0.057	–
DESI BAO+Union3	0.309 ± 0.013	9835 ± 140	$-0.811^{+0.079}_{-0.070}$	–
DESI BAO+DES-SN5YR	0.306 ± 0.012	9890 ± 100	-0.840 ± 0.052	–
GEDE				
DESI BAO	$0.296^{+0.014}_{-0.016}$	10170 ± 330	–	$0.12^{+0.81}_{-1.2}$
DESI BAO+PantheonPlus	0.299 ± 0.013	9993 ± 110	–	$-0.49^{+0.27}_{-0.32}$
DESI BAO+Union3	0.303 ± 0.014	9845 ± 140	–	$-0.86^{+0.30}_{-0.40}$
DESI BAO+DES-SN5YR	0.302 ± 0.014	9871 ± 99	–	$-0.80^{+0.24}_{-0.27}$
Mirage				
DESI BAO	$0.430^{+0.066}_{-0.044}$	8813^{+300}_{-630}	> 0.078	–
DESI BAO+PantheonPlus	0.311 ± 0.012	10010 ± 100	-0.880 ± 0.065	–
DESI BAO+Union3	0.331 ± 0.015	9768 ± 150	-0.67 ± 0.11	–
DESI BAO+DES-SN5YR	0.322 ± 0.011	9875 ± 99	-0.770 ± 0.073	–

[4] R. Calderon et al., *DESI 2024: Reconstructing Dark Energy using Crossing Statistics with DESI DR1 BAO data*, 2405.04216.

[5] E.V. Linder, *The Mirage of w=-1*, 0708.0024.

[6] DESI Collaboration, A.G. Adame, J. Aguilar, S. Ahlen, S. Alam, D.M. Alexander et al., *DESI 2024 III: Baryon Acoustic Oscillations from Galaxies and Quasars*, *arXiv e-prints* (2024) arXiv:2404.03000 [2404.03000].

[7] DESI Collaboration, A.G. Adame, J. Aguilar, S. Ahlen, S. Alam, D.M. Alexander et al., *DESI 2024 IV: Baryon Acoustic Oscillations from the Lyman Alpha Forest*, *arXiv e-prints* (2024)

arXiv:2404.03001 [2404.03001].

[8] M. Chevallier and D. Polarski, *Accelerating Universes with Scaling Dark Matter*, *International Journal of Modern Physics D* **10** (2001) 213 [gr-qc/0009008].

[9] R.R. Caldwell and E.V. Linder, *The Limits of quintessence*, *Phys. Rev. Lett.* **95** (2005) 141301 [astro-ph/0505494].

[10] J.A. Frieman, C.T. Hill, A. Stebbins and I. Waga, *Cosmology with ultralight pseudo Nambu-Goldstone bosons*, *Phys. Rev. Lett.* **75** (1995) 2077 [astro-ph/9505060].

[11] A. Linde, *Inflation and quantum cosmology.*, in *Three Hundred Years of Gravitation*, pp. 604–630 (1987).

[12] E.V. Linder, *Quintessence's last stand?*, *Phys. Rev. D* **91** (2015) 063006 [1501.01634].

[13] E.V. Linder, *The Dynamics of Quintessence, The Quintessence of Dynamics*, *Gen. Rel. Grav.* **40** (2008) 329 [0704.2064].

[14] L. Parker and A. Raval, *New quantum aspects of a vacuum dominated universe*, *Phys. Rev. D* **62** (2000) 083503 [gr-qc/0003103].

[15] R.R. Caldwell, W. Komp, L. Parker and D.A.T. Vanzella, *A Sudden gravitational transition*, *Phys. Rev. D* **73** (2006) 023513 [astro-ph/0507622].

[16] A. Banihashemi, N. Khosravi and A.H. Shirazi, *Ginzburg-Landau Theory of Dark Energy: A Framework to Study Both Temporal and Spatial Cosmological Tensions Simultaneously*, *Phys. Rev. D* **99** (2019) 083509 [1810.11007].

[17] A. Banihashemi, N. Khosravi and A. Shafieloo, *Dark energy as a critical phenomenon: a hint from Hubble tension*, *JCAP* **06** (2021) 003 [2012.01407].

[18] X. Li and A. Shafieloo, *A Simple Phenomenological Emergent Dark Energy Model can Resolve the Hubble Tension*, *Astrophys. J. Lett.* **883** (2019) L3 [1906.08275].

[19] S. Pan, W. Yang, E. Di Valentino, A. Shafieloo and S. Chakraborty, *Reconciling H_0 tension in a six parameter space?*, *JCAP* **06** (2020) 062 [1907.12551].

[20] X. Li and A. Shafieloo, *Evidence for Emergent Dark Energy*, *Astrophys. J.* **902** (2020) 58 [2001.05103].

[21] W. Yang, E. Di Valentino, S. Pan, A. Shafieloo and X. Li, *Generalized emergent dark energy model and the Hubble constant tension*, *Phys. Rev. D* **104** (2021) 063521 [2103.03815].

[22] M.J. Francis, G.F. Lewis and E.V. Linder, *Power Spectra to 1% Accuracy between Dynamical Dark Energy Cosmologies*, *Mon. Not. Roy. Astron. Soc.* **380** (2007) 1079 [0704.0312].

[23] DESI Collaboration, A. Aghamousa, J. Aguilar, S. Ahlen, S. Alam, L.E. Allen et al., *The DESI Experiment Part I: Science,Targeting, and Survey Design*, *arXiv e-prints* (2016) arXiv:1611.00036 [1611.00036].

[24] DESI Collaboration, B. Abareshi, J. Aguilar, S. Ahlen, S. Alam, D.M. Alexander et al., *Overview of the Instrumentation for the Dark Energy Spectroscopic Instrument*, *AJ* **164** (2022) 207 [2205.10939].

[25] DESI Collaboration, A.G. Adame, J. Aguilar, S. Ahlen, S. Alam, G. Aldering et al., *Validation of the Scientific Program for the Dark Energy Spectroscopic Instrument*, *AJ* **167** (2024) 62 [2306.06307].

[26] DESI Collaboration, A.G. Adame, J. Aguilar, S. Ahlen, S. Alam, G. Aldering et al., *The Early Data Release of the Dark Energy Spectroscopic Instrument*, *arXiv e-prints* (2023) arXiv:2306.06308 [2306.06308].

[27] DESI Collaboration, *DESI 2024 I: Data Release 1 of the Dark Energy Spectroscopic Instrument*, *in preparation* (2025) .

[28] DESI Collaboration, *DESI 2024 II: Sample definitions, characteristics and two-point clustering statistics*, in preparation (2024) .

[29] DESI Collaboration, *DESI 2024 V: Analysis of the full shape of two-point clustering statistics from galaxies and quasars*, in preparation (2024) .

[30] DESI Collaboration, *DESI 2024 VII: Cosmological constraints from full-shape analyses of the two-point clustering statistics measurements*, in preparation (2024) .

[31] D. Brout et al., *The Pantheon+ Analysis: Cosmological Constraints*, Astrophys. J. **938** (2022) 110 [2202.04077].

[32] D. Rubin et al., *Union Through UNITY: Cosmology with 2,000 SNe Using a Unified Bayesian Framework*, 2311.12098.

[33] DES collaboration, *The Dark Energy Survey: Cosmology Results With ~1500 New High-redshift Type Ia Supernovae Using The Full 5-year Dataset*, 2401.02929.

[34] PLANCK collaboration, *Planck 2018 results. VI. Cosmological parameters*, Astron. Astrophys. **641** (2020) A6 [1807.06209].

[35] PLANCK collaboration, *Planck 2018 results. V. CMB power spectra and likelihoods*, Astron. Astrophys. **641** (2020) A5 [1907.12875].

[36] J. Torrado and A. Lewis, *Cobaya: Code for Bayesian Analysis of hierarchical physical models*, J. Cosmology Astropart. Phys. **05** (2021) 057 [2005.05290].

[37] J. Carron, M. Mirmelstein and A. Lewis, *CMB lensing from Planck PR4 maps*, JCAP **09** (2022) 039 [2206.07773].

[38] M.S. Madhavacheril, F.J. Qu, B.D. Sherwin, N. MacCrann, Y. Li, I. Abril-Cabezas et al., *The Atacama Cosmology Telescope: DR6 Gravitational Lensing Map and Cosmological Parameters*, 2023.

[39] ACT collaboration, *The Atacama Cosmology Telescope: A Measurement of the DR6 CMB Lensing Power Spectrum and Its Implications for Structure Growth*, Astrophys. J. **962** (2024) 112 [2304.05202].

[40] A. Lewis and S. Bridle, *Cosmological parameters from CMB and other data: A Monte Carlo approach*, Phys. Rev. **D66** (2002) 103511 [astro-ph/0205436].

[41] A. Lewis, *Efficient sampling of fast and slow cosmological parameters*, Phys. Rev. **D87** (2013) 103529 [1304.4473].

[42] R.M. Neal, *Taking Bigger Metropolis Steps by Dragging Fast Variables*, ArXiv Mathematics e-prints (2005) [math/0502099].

[43] J. Lesgourgues, *The Cosmic Linear Anisotropy Solving System (CLASS) I: Overview*, arXiv e-prints (2011) arXiv:1104.2932 [1104.2932].

[44] D. Blas, J. Lesgourgues and T. Tram, *The Cosmic Linear Anisotropy Solving System (CLASS). Part II: Approximation schemes*, J. Cosmology Astropart. Phys. **2011** (2011) 034 [1104.2933].

[45] E.V. Linder, *Mapping the Cosmological Expansion*, Rept. Prog. Phys. **71** (2008) 056901 [0801.2968].

[46] D. Shlivko and P. Steinhardt, *Assessing observational constraints on dark energy*, 2405.03933.

[47] W.J. Handley, M.P. Hobson and A.N. Lasenby, *PolyChord: nested sampling for cosmology*, Mon. Not. Roy. Astron. Soc. **450** (2015) L61 [1502.01856].

[48] W. Handley, *anesthetic: nested sampling visualisation*, J. Open Source Softw. **4** (2019) 1414 [1905.04768].

[49] H. Jeffreys, *The Theory of Probability*, Oxford Classic Texts in the Physical Sciences (1939).

[50] R. Trotta, *Applications of Bayesian model selection to cosmological parameters*, *Mon. Not. Roy. Astron. Soc.* **378** (2007) 72 [`astro-ph/0504022`].

[51] H. Dembinski and P.O. et al., *scikit-hep/iminuit*, Dec, 2020. 10.5281/zenodo.3949207.

[52] C. Cartis, J. Fiala, B. Marteau and L. Roberts, *Improving the flexibility and robustness of model-based derivative-free optimization solvers*, `1804.00154`.

[53] C. Cartis, L. Roberts and O. Sheridan-Methven, *Escaping local minima with local derivative-free methods: a numerical investigation*, *Optimization* **71** (2021) 2343–2373.

[54] H. Koo, R.E. Keeley, A. Shafieloo and B. L'Huillier, *Bayesian vs frequentist: comparing Bayesian model selection with a frequentist approach using the iterative smoothing method*, *JCAP* **03** (2022) 047 [`2110.10977`].

[55] R.E. Keeley and A. Shafieloo, *On the distribution of Bayesian evidence*, *Mon. Not. Roy. Astron. Soc.* **515** (2022) 293 [`2111.04231`].

[56] A. Lewis, *GetDist: a Python package for analysing Monte Carlo samples*, `1910.13970`.

[57] C.R. Harris, K.J. Millman, S.J. van der Walt, R. Gommers, P. Virtanen, D. Cournapeau et al., *Array programming with NumPy*, *Nature* **585** (2020) 357.

[58] P. Virtanen, R. Gommers, T.E. Oliphant, M. Haberland, T. Reddy, D. Cournapeau et al., *SciPy 1.0: Fundamental Algorithms for Scientific Computing in Python*, *Nature Methods* **17** (2020) 261.

[59] J.D. Hunter, *Matplotlib: A 2d graphics environment*, *Computing in Science & Engineering* **9** (2007) 90.

C Author Affiliations

[1]Korea Astronomy and Space Science Institute, 776, Daedeokdae-ro, Yuseong-gu, Daejeon 34055, Republic of Korea

[2]University of Science and Technology, 217 Gajeong-ro, Yuseong-gu, Daejeon 34113, Republic of Korea

[3]Lawrence Berkeley National Laboratory, 1 Cyclotron Road, Berkeley, CA 94720, USA

[4]Space Sciences Laboratory, University of California, Berkeley, 7 Gauss Way, Berkeley, CA 94720, USA

[5]University of California, Berkeley, 110 Sproul Hall #5800 Berkeley, CA 94720, USA

[6]Departamento de Física, Instituto Nacional de Investigaciones Nucleares, Carreterra México-Toluca S/N, La Marquesa, Ocoyoacac, Edo. de México C.P. 52750, México

[7]IRFU, CEA, Université Paris-Saclay, F-91191 Gif-sur-Yvette, France

[8]Instituto de Física Teórica (IFT) UAM/CSIC, Universidad Autónoma de Madrid, Cantoblanco, E-28049, Madrid, Spain

[9]Department of Physics, The University of Texas at Dallas, Richardson, TX 75080, USA

[10]Physics Dept., Boston University, 590 Commonwealth Avenue, Boston, MA 02215, USA

[11]Department of Physics & Astronomy, University College London, Gower Street, London, WC1E 6BT, UK

[12]Instituto de Física, Universidad Nacional Autónoma de México, Cd. de México C.P. 04510, México

[13]NSF NOIRLab, 950 N. Cherry Ave., Tucson, AZ 85719, USA

[14]Department of Physics & Astronomy and Pittsburgh Particle Physics, Astrophysics, and Cosmology Center (PITT PACC), University of Pittsburgh, 3941 O'Hara Street, Pittsburgh, PA 15260, USA

[15]Departamento de Física, Universidad de los Andes, Cra. 1 No. 18A-10, Edificio Ip, CP 111711, Bogotá, Colombia

[16]Observatorio Astronómico, Universidad de los Andes, Cra. 1 No. 18A-10, Edificio H, CP 111711 Bogotá, Colombia

[17]Institut d'Estudis Espacials de Catalunya (IEEC), 08034 Barcelona, Spain

[18]Institute of Cosmology and Gravitation, University of Portsmouth, Dennis Sciama Building, Portsmouth, PO1 3FX, UK

[19]Institute of Space Sciences, ICE-CSIC, Campus UAB, Carrer de Can Magrans s/n, 08913 Bellaterra, Barcelona, Spain

[20]School of Mathematics and Physics, University of Queensland, 4072, Australia

[21]Department of Astronomy and Astrophysics, University of Chicago, 5640 South Ellis Avenue, Chicago, IL 60637, USA

[22]Fermi National Accelerator Laboratory, PO Box 500, Batavia, IL 60510, USA

[23]Sorbonne Université, CNRS/IN2P3, Laboratoire de Physique Nucléaire et de Hautes Energies (LPNHE), FR-75005 Paris, France

[24]Center for Cosmology and AstroParticle Physics, The Ohio State University, 191 West Woodruff Avenue, Columbus, OH 43210, USA

[25]Department of Astronomy, The Ohio State University, 4055 McPherson Laboratory, 140 W 18th Avenue, Columbus, OH 43210, USA

[26]The Ohio State University, Columbus, 43210 OH, USA

[27]Institució Catalana de Recerca i Estudis Avançats, Passeig de Lluís Companys, 23, 08010 Barcelona, Spain

[28]Institut de Física d'Altes Energies (IFAE), The Barcelona Institute of Science and Technology, Campus UAB, 08193 Bellaterra Barcelona, Spain

[29]Department of Physics and Astronomy, Siena College, 515 Loudon Road, Loudonville, NY 12211, USA

[30]Departamento de Física, Universidad de Guanajuato - DCI, C.P. 37150, Leon, Guanajuato, México

[31]Instituto Avanzado de Cosmología A. C., San Marcos 11 - Atenas 202. Magdalena Contreras, 10720. Ciudad de México, México

[32]Department of Physics and Astronomy, University of Waterloo, 200 University Ave W, Waterloo, ON N2L 3G1, Canada

[33]Perimeter Institute for Theoretical Physics, 31 Caroline St. North, Waterloo, ON N2L 2Y5, Canada

[34]Waterloo Centre for Astrophysics, University of Waterloo, 200 University Ave W, Waterloo, ON N2L 3G1, Canada

[35]Instituto de Astrofísica de Andalucía (CSIC), Glorieta de la Astronomía, s/n, E-18008 Granada, Spain

[36]Department of Physics and Astronomy, Sejong University, Seoul, 143-747, Korea

[37]CIEMAT, Avenida Complutense 40, E-28040 Madrid, Spain

[38]Space Telescope Science Institute, 3700 San Martin Drive, Baltimore, MD 21218, USA

[39]Department of Physics, University of Michigan, Ann Arbor, MI 48109, USA

[40]University of Michigan, Ann Arbor, MI 48109, USA

[41]Department of Physics & Astronomy, Ohio University, Athens, OH 45701, USA

[42]National Astronomical Observatories, Chinese Academy of Sciences, A20 Datun Rd., Chaoyang District, Beijing, 100012, P.R. China